The UV Spectrum of the Lyman-Birge-Hopfield Band System of N_2 Induced by Cascading from Electron Impact

Joseph M. Ajello[1], J. Scott Evans[2], Victoir Veibell[2], Charles P. Malone[3], Greg M. Holsclaw[1], Alan C. Hoskins[1], Rena A. Lee[1,a], William E. McClintock[1], Saurav Aryal[1], Richard W. Eastes[1], and Nicholas Schneider[1]

[1]*Laboratory for Atmospheric and Space Physics, University of Colorado, Boulder, CO 80303*
[2]*Computational Physics Inc., Springfield, VA 22151*
[3]*Jet Propulsion Laboratory, California Institute of Technology, Pasadena, CA 91109*
[a]*Vassar College, Poughkeepsie, NY 12604*

Journal of Geophysical Research — Space Physics

November 13, 2019

4294 Words
2 Tables
7 Figures

Key Points:

- First imaging measurement of the electron-impact N_2 LBH cascade-induced spectrum at energies of 30–200 eV is presented.
- Cascading transition to the N_2 *a*-state (a' & $w \rightarrow a$) from radiative & collision-induced-electronic transitions (CIETs).
- We present measurement of vibrational LBH band intensities between 30–200 eV at various pressures and electron impact direct and cascade LBH emission cross-sections between 40–200 eV.

Index Terms: 0310/5408 Airglow and Aurora; 0343 Planetary Atmospheres; 0358/3369 Thermosphere: energy deposition; 2423, Ionosphere processes; 6225, Mars; 6281 Titan.

Key Words: molecular nitrogen (N_2); Lyman-Birge-Hopfield (LBH) band system; electron impact; fluorescence cascade; MAVEN IUVS, GOLD, collision-induced-electronic-transitions.

Abstract

We have measured in the laboratory the far ultraviolet (FUV: 125.0–170.0 nm) cascade-induced spectrum of the Lyman-Birge-Hopfield (LBH) band system ($a\,^1\Pi_g \rightarrow X\,^1\Sigma_g^+$) of N_2 excited by 30–200 eV electrons. The cascading transition begins with two processes: radiative and collision-induced electronic transitions (CIETs) involving two states ($a'\,^1\Sigma_u^-$ and $w\,^1\Delta_u \rightarrow a\,^1\Pi_g$), which are followed by a cascade induced transition $a\,^1\Pi_g \rightarrow X\,^1\Sigma_g^+$. Direct excitation to the *a*-state produces a confined LBH spectral glow pattern around an electron beam. We have spatially resolved the electron induced glow pattern from an electron beam colliding with N_2 at radial distances of 0–400 mm at three gas pressures. This imaging measurement is the first to isolate spectral measurements in the laboratory of single-scattering electron-impact-induced-fluorescence from two LBH emission processes: direct excitation, which is strongest in emission near the electron beam axis; and cascading-induced, which is dominant far from the electron beam axis. The vibrational populations for vibrational levels from v′=0–2 of the $a\,^1\Pi_g$ state are enhanced by CIETs, and the emission cross sections of the LBH band system for direct and cascading-induced excitation are provided at 40, 100, and 200 eV.

1. Introduction

The study of the Lyman-Birge-Hopfield (LBH) band system ($a\,^1\Pi_g \rightarrow X\,^1\Sigma_g^+$) of N_2 in the laboratory by UV spectroscopy has heretofore failed to measure the cascade-induced UV spectrum and determine LBH vibrational intensities or cascade emission cross sections. This failure has precipitated a controversy in the literature that has persisted for over a decade due to the dichotomy between terrestrial airglow observations and model calculations [*Cartwright,* 1978; *Budzien et al.,* 1994; *Eastes and Dentamaro,* 1996; *Eastes,* 2000]. Analysis of terrestrial far ultraviolet (FUV) airglow spectra is aimed at determining the abundances of the major constituents of the upper thermosphere: N_2, O_2, and O. The retrieval of thermospheric column abundance ratio O/N_2 (also referred to as $\Sigma\,O/N_2$ in the literature) depends upon N_2 LBH and O emission cross sections [*Strickland et al.,* 1995, 1999; *Evans et al.,* 1995]. The relative vibrational distributions of the LBH band system observed in the dayglow and aurora sometimes agree with theoretical calculations for direct impact [*Ajello,* 1970; *Ajello and Shemansky,* 1985] and other times statistically significant departures of 30–50% occur [*Budzien et al.,* 1994; *Eastes and Dentamaro,* 1996; *Ajello et al.,* 2011]. We can thus shed light on the origin of the difference in the UV spectrum between laboratory and space-borne measurements. The principal cause is the pressure-dependent lifetimes and energy-dependent cross sections for cascade to the *a*-state from the ($a'\,^1\Sigma_u^-$ and $w\,^1\Delta_u \rightarrow a\,^1\Pi_g \rightarrow X\,^1\Sigma_g^+$) states by two separate processes: radiative *and* collision-induced-electronic transitions (CIETs).

The $a\,^1\Pi_g$ state is itself metastable from direct excitation being magnetic dipole and electric quadrupole in character. Due to the ~50 μs lifetime of the *a*-state, a molecule excited directly to the $a\,^1\Pi_g$ state can travel ~1000 cm without a molecular collision (either elastic or inelastic) at the lowest pressures measured here (and more importantly, only up to 10 cm to the 99.7% 3σ-level

before radiating) [*Marinelli et al.,* 1989; *Ajello et al.,* 2017]. The lifetimes of the cascade states are markedly longer requiring a large vacuum system to observe and fully measure both forbidden radiation sources. Our imaging experiment is the first to measure and isolate the optical emissions of single-scattering (i.e., low-pressure) electron-impact-induced-fluorescence from both direct excitation of the $a\,^1\Pi_g$ state and cascade-induced fluorescence contributions to the $a\,^1\Pi_g$ state. There is marked difference between the *a′*-state and *w*-state lifetimes to the ground state. The *a′*-state lifetime is found to be ~40 ms by *Wilkinson and Tilford* [1959], while *Tilford and Benesch* [1976] find the lifetime to be ~13 ms for v′=0, noting that *a′*(0) energetically resides below *a*(0). More recently, *Eastes and Dentamaro* [1996] recommend a lifetime of ~17 ms for the $a'\,^1\Sigma_u^- \rightarrow X\,^1\Sigma_g^+$ forbidden transition (that proceeds through nearby $^1\Pi_u$ states). The *w*-state is dipole forbidden from the ground state and can only be depopulated by CIET or radiative cascade decay to the *a*-state with a radiative lifetime to the ground state on the order of seconds for the forbidden $w\,^1\Delta_u \rightarrow X\,^1\Sigma_g^+$ transition. In this paper, we discuss the dipole-allowed transitions ($a'\,^1\Sigma_u^-$ and $w\,^1\Delta_u \rightarrow a\,^1\Pi_g$) in Section 3. We also present measurement results of LBH vibrational band intensities from 30–200 eV at different pressures and provide electron impact cross sections for cascade and direct excitation of LBH at 40–200 eV energy range.

2. Experimental Apparatus

In the past we have constructed a large (1.5 m-diameter) vacuum system apparatus for measuring the emission cross sections of the strongest optically forbidden transitions found in a solar system planetary atmosphere airglow: N_2 LBH [*Ajello et al.*, 2017], O I 135.6 nm from O_2 [*Noren et al.,* 2001; *Kanik et al.,* 2003], and O I 135.6 nm from CO and CO_2 [*Ajello et al.,* 2019], as well as the Cameron bands from CO and CO_2 in the middle ultraviolet (MUV) [*Lee et al.,* 2019].

Using the aforementioned large vacuum chamber housing an electron gun system and the Mars Atmosphere and Volatile EvolutioN (MAVEN) mission Imaging UltraViolet Spectrograph (IUVS) optical engineering model (OEM) instrument, we have obtained calibrated spectral measurements of the LBH band system from 125–175 nm over a range of lines-of-sight to capture most of the optical emissions within the LBH band system [*McClintock et al.,* 2014]. The experimental apparatus for emission cross sections has been discussed in detail previously [*Noren et al.*, 2001; *Kanik et al.*, 2003; *Ajello et al.,* 2017].

The experiment reported here for N_2 passed an electron beam through a static gas at three different pressures: 5×10^{-6} Torr, 1×10^{-5} Torr, and 5×10^{-5} Torr, hereafter low, medium, and high, respectively, corresponding to N_2 abundances in the terrestrial atmosphere at altitudes of 125 km ($n=1.8 \times 10^{11}$ cm^{-3}), 120 km ($n=3.5 \times 10^{11}$ cm^{-3}), and 110 km ($n=1.8 \times 10^{12}$ cm^{-3}). The IUVS-OEM measured the glow profile produced around the electron beam. Ideally, an infinitely long electron beam will produce a cylindrically uniform glow region, wherein single-scattering emission and excitation rates per unit length of the beam are equal with dipole-allowed electronic transitions occurring on the electron beam axis and metastable transitions forming an extended cylindrically symmetric glow. A large vacuum chamber, referred to as the Multi-Optical Beam Instrument (MOBI), is large enough to approximate this condition with its 1.5 m diameter girth and 2.35 m length. In the present work, the IUVS-OEM instrument was placed on a vertical moving stage with the entrance slit orthogonal to the electron beam table, peering at the electron beam up to 400 mm from the electron beam axis to fully measure both allowed and forbidden transitions. The electron-impact-fluorescence apparatus installed in the MOBI chamber consisted of an electrostatic electron gun source and Faraday cup separated by ~1/3-m, two large pair of

Helmholtz coils surrounding the chamber, a static gas source, and the IUVS-OEM. The apparatus is described fully and shown schematically in Fig. 2 of *Ajello et al.* [2017].

With a staged 3-step motion, the field-of-view (FOV) of the IUVS-OEM detector was projected to more than 400 mm object distance at the electron beam allowing the observation of metastable emissions. Three overlapping images were taken at different stage positions to capture the glow region from long-lived states such as N_2 $a\,^1\Pi_g$. We can vary the vertical height of the placement of the optic axis of the IUVS-OEM at three positions above the electron beam axis. We start from Image-1 on center (z = 0) with the emission from dipole-allowed transitions centered near spatial pixel 500, followed by a motion in the z-direction to obtain Image-2 centered at 15.24 cm (6 inches), and Image-3 centered at 30.48 cm (12 inches) above the electron beam. The total vertical object size in the MOBI chamber imaged by the central 810 spatial pixels of the IUVS-OEM is 16.4 cm with Image-1 positioned at the center of the FOV. The same set of three spatial image positions are used at low, medium, and high pressure. The set of 810 pixels used is a subset of the full 1024 pixels and is chosen to avoid the pixels of the broad occultation keyholes at each end of the slit, which are used on the flight instrument for stellar occultation observations.

Our main discussion in this paper involves an analysis of the best-fit LBH vibrational intensities for the Image-1 and Image-3 laboratory measured spectra, e.g., Image-1 low pressure or Image-1 high pressure compared to Image-3 high pressure. These conditions present different spectra, as evidenced in Fig. 1, where we have over-plotted the high-pressure spectra for Image-1 and Image-3 with both spectra normalized to the $a(3,0)$ band at 135.4 nm. Multiple Linear Regression (MLR) glow model fits to the measured 100 eV medium and high pressure FUV intensities for the portion of the LBH spectrum from 133.5–140.2 nm, a spectral region devoid of N I features, are shown in Figs. 2a and 2b, respectively. Both sets of glow patterns show that only

Image-1 captures a direct excitation spectrum with termination of direct excitation photons in the model, shown in green near 10 cm radial distance from the electron beam. The Image-3 glow pattern in the model, shown in magenta captures the cascade-induced LBH spectrum, which dominates from radial distances of 22.5–38.5 cm.

An important diagnostic of the IUVS-OEM optical performance in the laboratory requires a measurement of the point-spread function (PSF). To obtain the PSF, the MOBI chamber background gas consisting of predominantly H_2O, following pump-down, was sampled at an approximately static pressure of ~7×10^{-6} Torr for a short duration and the electron gun provided an electron beam current of ~30 μA. The FUV spectrum of electron impact fluorescence of H_2O is very simple, comprised of mostly H I Lyman-α and O I (115.2, 130.4, and 135.6 nm) emission features [*Ajello et al.,*1985]. The model fit, *f*, to the PSF is given in *Ajello et al.* [2019].

3. The Spectral Analysis

For diatomic molecules in an electronically excited state, the number of photons emitted per unit volume per second in a transition from the v′ upper vibrational level to the v″ lower vibrational level [*Beegle et al.,* 1999], referred to as the electronic band emission rate, is

$$I_{v'v''} = p_{v'} A_{v'v''} / A_{v'}, \quad (1)$$

where $p_{v'}$ is the volumetric excitation rate for the v′ level of the upper electronic state, and $A_{v'v''}$ and $A_{v'}$ are the vibrational and total transitional probabilities for each v′ level to a lower electronic state. The value $p_{v'}$ is defined by

$$p_{v'} = F_e N_0 (\sigma_{excitation}^{v'} + \sigma_{cascade}^{v'}), \quad (2)$$

where F_e is the electron flux, N_0 is the gas density (cm^{-3}), $\sigma_{excitation}^{v'}$ is the excitation cross section (cm^2), and $\sigma_{cascade}^{v'}$ is the total cascade cross section (cm^2) to level v′ of the *a*-state from various

vibrational levels of the *a′*- and *w*-states. Note that $\sigma_{excitation}^{v'}$ is proportional to $q_{v'0}\,R_e^2(r_{v'0})$, where $q_{v'0}$ is the Franck-Condon factor (FCF) from ground vibrational level to v′, $r_{v'0}$ is the corresponding internuclear distance, and R_e^2 is the square of the electronic transition moment. Also note that we have previously shown dipole-allowed cascade from three Rydberg series, with lowest members $b\ ^1\Pi_u$, $c_3\ ^1\Pi_u$, $o_3\ ^1\Pi_u$, $b'\ ^1\Sigma_u^+$, and $c_4'\ ^1\Sigma_u^+$, as well as valence-type states, is small [*Heays et al.,* 2013]. There is less than 5% variation of the electronic transition moment, R_e, of the *a*-state [*Ajello,* 1970], so the variation of R_e with internuclear distance can be neglected.

We use MLR techniques to fit an N_2 LBH band emission rate model [*Budzien et al.,* 1994] to each IUVS-OEM measurement obtained in our laboratory experiment. The PSF (discussed above) was used to spectrally smear individual molecular rotational lines to model the measured electron impact fluorescence FUV spectra. The measured laboratory temperature established the rotational temperature of 293 K when fitting spectra with the band model. With the exception of the N I 149.3 nm doublet, which was removed from the measured spectra prior to fitting, expected atomic multiplets (N, H, and O, the latter two resulting from residual gas in the tank) were included as source components in the fits. Uncertainties in the measured spectra are propagated through the MLR fit when obtaining coefficients (i.e., v′-vibrational populations) and their corresponding uncertainty estimates. In Table 1 we list the MLR band emission rate model results for the six spectra of Images-1 and -3. The observed pre-dissociation of the a-state for rotational levels above v′=6, J=13, accounts for 12.3% of the excitation cross section resulting in emission from v′>6 to be weak or absent [*Ajello,* 1970]. Thus, the total probability for emission for all columns in Table 1 has been normalized to $\sum_{v'}^{6} q_{v'0} = 0.877$.

In Fig. 3a (bottom abscissa, left ordinate) we show the IUVS-OEM electron-excited 30 eV Image-1 laboratory spectra at a radial distance of 0 cm from the electron beam for low and high

192 pressure. The spectra are normalized to the LBH *a*(3,0) band at 135.4 nm. Also shown in the figure
193 (top abscissa, right ordinate) is a comparison of direct excitation theoretical Franck-Condon
194 factors, $q_{v'0}$, from *Loftus and Krupenie*, [1977] with vibrational intensities for each v′ (0,1,2,…,6),
195 v″-progression from MLR fits to Image-1 spectra at low and high pressure, and a fit to the Image-
196 3 spectrum at high pressure. The low v′ levels 0, 1, and 2 are enhanced in Image-3, which exhibits
197 a cascade spectrum for a gas pressure of 5×10^{-5} Torr, equivalent to an N_2 gas density of
198 1.8×10^{12} cm^{-3}. The enhancement of the strong *a*(1,1) band at 146.4 nm is very noticeable in Fig.
199 1. This N_2 density occurs at terrestrial altitudes near 110–115 km, well below the peak of the LBH
200 emission rate near 150 km. The v′=0 level is the most enhanced by combined CIET and radiative
201 processes by almost 50% when comparing vibrational intensities for Image-1 and Image-3 at high
202 pressure.

203 The results of an MLR analysis comparing vibrational intensities of Image-3 at low,
204 medium, and high pressures are shown in Fig. 3b (top abscissa, right ordinate). IUVS-OEM
205 electron-excited 30 eV Image-3 laboratory spectra at a radial distance of 30.48 cm from the
206 electron beam for medium and high pressures are also shown (bottom abscissa, left ordinate). The
207 spectra are normalized to the LBH *a*(3,0) band at 135.4 nm. The airglow observations reported by
208 *Budzien et al.* [1994] and the CIET model results of *Eastes* [2000], expected for airglow rocket
209 observations at a tangent altitude of 200 km, indicate similar enhancements in the low vibrational
210 levels evident in our Image-3 high-pressure spectrum. We expect to see this enhancement in any
211 N_2 FUV limb spectra of the dayglow at the reference altitudes used in our laboratory experiment.
212 Even in the absence of a significant collision rate (e.g., ~0.1 s^{-1}) as expected near 200 km
213 (n~3.6×10^9 cm^{-3}), the radiative induced-cascade from the $a'\,^1\Sigma_u^-$ and $w\,^1\Delta_u \rightarrow a\,^1\Pi_g \rightarrow X\,^1\Sigma_g^+$)
214 states will take place in our experiment with a larger transition probability (~10^3 s^{-1}) than the

collision rate due to deactivation that takes place in the lab with a small chamber [*Gilmore et al.,* 1992].

Low-v′ enhancement for medium and high pressures was recognized in the LBH intensity versus pressure variation studies in the work of *Ajello* [*1970*] and *Holland* [*1969*] with a small vacuum chamber compared to the MOBI chamber at UC. In these earlier experiments, only *Image-1*-type spectra were possible, requiring higher pressures to see CIET than obtained here for our low-pressure Image-3 measurements.

The strength of the radiative-CIET cascade process induced low-v′ enhancement is expected to increase with gas pressure. This is because the CIET process, strictly speaking, is a secondary collision in this experiment via the processes in Eq. 3 between excited states, but is not, strictly speaking, single-scattering:

$$N_2(a'\,^1\Sigma_u^-, w\,^1\Delta_u, a\,^1\Pi_g) + N_2(X\,^1\Sigma_g^+) \leftrightarrow N_2(a'\,^1\Sigma_u^-, w\,^1\Delta_u, a\,^1\Pi_g) + N_2(X\,^1\Sigma_g^+). \quad (3)$$

Eastes and Dentamarro [1996] and *Freund* [1972] have indicated that the following radiative and CIET collisions occur interchangeably: $a \leftrightarrow a'$, $w \leftrightarrow a$, with no coupling between the *w*- and *a′*-states. *Marinelli et al.,* [1989] and *Katayama et al.* [1994] have shown a strong exothermic reaction for $a(v'=0) \rightarrow a'(v'=0)$ should be the dominant contribution to the CIET rate constant as we verify in this experiment.

4. Discussion

In order to demonstrate the separation of the two types of LBH spectra, we performed a best-fit MLR for the 100 eV medium and high-pressure glow patterns employing a direct excitation lifetime and a composite cascading lifetime as in Fig. 2. Direct excitation becomes insignificant (<1%) at distances greater than 10 cm from the electron beam. We found a similar result for all energies from 30–200 eV. The regression analysis showed a physically meaningful

direct excitation model for the fast component lifetime of ~50 μs and ~5000 μs for the cascade-induced LBH spectrum, similar to the 100 eV spectrum studied in *Ajello et al.* [2017]. The observed ratio of direct excitation to cascade-induced excitation to the *a*-state in this experiment is nominally ~70% to ~30% for all energies above 30 eV.

Direct excitation observed in the set of three Image-1 at all pressures for all our laboratory spectra at 30 eV are nearly identical and can all be closely modeled with Franck-Condon factors. Cascading processes observed in Image-3 at high pressure result in a large increase in the LBH emission intensity at electron collision energies of 10~200 eV, which also corresponds to the typical energy range for secondary electrons in Earth's upper atmosphere. The LBH band emission rate from cascade varies with gas pressure with main enhancement to low v′ levels. The cross section for cascading-induced LBH emission is found to be pressure dependent and also energy dependent as discussed in the past [*Eastes and Dentamaro*, 1996]. We show in Fig. 4 the relative LBH vibrational band intensities for Image-3 as a function of energy normalized to 0.877, the sum of FCF ($q_{v'0}$) for emission. CIET effects become stronger with increasing energy for the sum of Images-1–3 at high pressure. The trend in fitted populations for v′=6 is not understood at present and will require further investigation.

We display in Fig. 5 and tabulate in Table 2 the variation of LBH direct emission cross section and LBH cascade-induced emission cross section with energy measured in this experiment at 40, 100, and 200 eV at medium pressure. The N_2 LBH emission cross section at each energy is normalized relative to the N I 120.0 nm emission cross sections of *Young et al.* [2010] with the correction factor suggested by *Malone et al.* [2008]: at 100 eV, $\sigma_{120.0\,nm} = 3.70 \times 10^{-18}$ cm^2. The medium pressure LBH direct-emission and cascade-emission cross sections in Table 2 are averaged based on the 100 eV direct LBH emission cross section results of *Ajello et al.* [2017] for

100 eV of 6.4×10^{-18} cm^2 and the 100 eV direct LBH emission value measured in this new experiment at medium pressure of 4.3×10^{-18} cm^2, resulting in a 100 eV LBH direct emission cross section of 5.4×10^{-18} cm^2. These averaged emission cross section results in Table 2 show cascading accounts for ~30% ($\sigma^{em}_{casc} = 2.5 \times 10^{-18}$ cm^2) of the glow pattern, and direct excitation of the *a*-state provides ~70% of the LBH emission ($\sigma^{em}_{dir} = 5.4\times 10^{-18}$ cm^2, i.e., the typical 'laboratory' LBH cross-section for smaller FOV setups). Thus, the total LBH emission cross-section is $\sigma^{em}_{total} = 7.9\times 10^{-18}$ cm^2, which is effectively the 'aeronomical' LBH cross-section at 100 eV. We also list in Table 2 the LBH predissociation cross sections and excitation cross sections as calculated in Ajello et al. [2017].

The composite uncertainty of the 100 eV (LBH) band system ($a\,^1\Pi_g \rightarrow X\,^1\Sigma_g^+$) emission cross section values is ~35% including the statistical uncertainty of the signal-to-noise ratio (SNR). The uncertainty of our work is the root-sum-square uncertainty of: 1) ~15% in the relative FUV calibration, 2) ~13.5% uncertainty of the absolute calibration of N I 120.0 nm, 3) ~5% uncertainty in the Faraday cup current loss to the grounded shield, 4) ~5% uncertainty to pressure drift, 5) ~15% uncertainty in measured areas from blended feature overlap, 6) ~20% uncertainty for the cascade-induced emission beyond ~400 mm radius from electron beam, and 7) SNR statistical uncertainty of 10%.

We show the statistical uncertainties in Fig. 6 for Images 1–3 for the wavelength region of the spectrum used for the emission cross section determination. The SNR remains >5 for all three of the images in the wavelength range. This wavelength range of 133.5–140.0 nm contains only LBH bands representing ~13.5% of the band system without any contamination from atomic-N multiplets and we use the integrated intensity (i.e., intensities summed over positive z-translation above the electron beam from 0–400 mm) from this portion of the LBH band system to deduce the

cross section of the band system [*Ajello and Shemansky*, 1985]. The two strongest bands of the LBH system dominate this spectral range: the *a*(2,0) and *a*(5,3) bands at 138.3 nm and the *a*(3,0) and *a*(6,2) bands at 135.3 nm. In addition, we included in this interval the *a*(5,1) band at 133.9 nm and the *a*(6,3) and *a*(3,1) bands at 139.5 nm. We determine from glow models that we were able to measure >98% of the emitted photons in the 133.5–140.0 nm spectral interval that arise from direct excitation.

A recent example of the CIET effect in planetary atmospheres can be seen in MLR fits to observations by the GOLD instrument. Fig. 7 (top abscissa, right ordinate) shows vibrational intensities from MLR fits to limb FUV observations made on October 31, 2018. The observed spectra have been summed over three altitude ranges: 100–150 km, 150–200 km, and 200–250 km. Similar to the approach used for the laboratory-measured spectra, the GOLD PSF was used to spectrally smear individual molecular rotational lines to model the observed FUV spectra. When fitting the GOLD spectra, the effective rotational temperature (~840 K) was first obtained using Powell optimal estimation techniques. The observed spectra for the three altitude bins, normalized to the *a*(2,0) band at 138.3 nm, are also shown in Fig. 7 (bottom abscissa, left ordinate). As done with the laboratory-measured spectra, the N I 149.3 nm doublet was removed from the measured spectra prior to fitting; no atomic multiplets were included as source components in the fits. There is a clear low-v′ enhancement in all three altitude-bins, an indication of pressure dependent CIET effects.

5. Summary

We have measured the LBH cascade-induced spectra at 30–200 eV for three different N_2 gas pressures corresponding to terrestrial altitudes between 110 km and 125 km (airglow) and at three different imaging glow distances from the electron beam of 0, 15.24 (6 in), and 30.48 cm

307 (12 in). The cascade-induced UV spectra were obtained from an LBH glow laboratory
308 measurement generated by an electron beam in a large vacuum chamber. Image-1 solely contains
309 the electron beam spectrum, and Image-3 at 30.48 cm distance from the electron beam captures
310 only the cascade spectrum.

311 The LBH emission cross section variation with both pressure and energy must be further
312 studied at lower energy near to threshold (~8.55 eV) than the 40–200 eV energy range measured
313 here for input into state-of-the-art electron transport models for accurate dayglow and auroral
314 analysis. The previous low energy studies of the LBH direct emission cross section, albeit in a
315 small chamber, were performed by *Ajello and Shemansky* [1985] and *Young et al.* [2010]. We
316 show these excitation function measurements for direct emission in Fig. 5, normalized at 100 eV
317 to the direct emission cross section value of 0.54×10^{-17} cm^2 measured here. The revised *Ajello*
318 *and Shemansky* direct emission cross sections in Fig. 5 agree closely with the peak cross section
319 values tabulated in the review article of *Ajello et al.* [2011]. *Ajello et al.* [2011] indicate in their
320 Table 28.5 a peak total LBH direct emission cross section of 2.65×10^{-17} cm^2 at 18 eV. The review
321 article includes a discussion of the work of *Eastes* [2000] and *Budzien et al.* [1994] from terrestrial
322 dayglow observations. The latter two publications indicate peak total emission cross sections
323 including cascade-induced emission cross section of 2.9×10^{-17} cm^2 and 3.55×10^{-17} cm^2,
324 respectively. These total peak emission cross section values are in excellent agreement with the
325 peak value indicated in Fig. 5 for the revised work of *Ajello and Shemansky* of ~2.9×10^{-17} cm^2.
326 Until we can build an electrostatic gun that can operate at low electron acceleration energy of
327 <30 eV we recommend adoption of a 30% contribution to the total emission cross section from
328 cascade-induced LBH emission at all energies above ~30 eV, where vibrational level threshold
329 effects are negligible.

6. Acknowledgements

This work was performed at the Laboratory for Atmospheric and Space Physics (LASP), University of Colorado (CU) Boulder, and the Jet Propulsion Laboratory (JPL), California Institute of Technology (Caltech), under a contract with the National Aeronautics and Space Administration (NASA). We gratefully acknowledge financial support through NASA's Solar System Workings, Cassini Data Analysis Program, the Heliophysics HTIDES and Geospace Science programs, and the National Science Foundation Aeronomy Program Office. This research was also supported by NASA through the MAVEN project including the use of the IUVS-OEM. R. A. Lee thanks the NSF Research Experiences for Undergraduates (REU) program for support. We thank Karl Hubbell for technical support. The GOLD data used in this analysis are available through the NASA Space Physics Data Facility (https://cdaweb.gsfc.nasa.gov/pub/data/gold/). Other data used are listed in the references; otherwise, please email the corresponding author for data tables. Government sponsorship is acknowledged.

6. References

Aarts, J. F. M., and F. J. de Heer, Emission cross sections for NI and NII multiplets and some molecular bands for electron impact on N_2. *Physica*, **52**, 45-73 (1971).

Ajello, J. M., Emission cross sections of N_2 in the vacuum ultraviolet by electron impact. *J Chem. Phys*., **53**, 1156, (1970).

Ajello, J. M. and D. E. Shemansky, "A Re-examination of Important N_2 Cross Sections by Electron Impact with Application to the Dayglow: The Lyman-Birge Hopfield Band System and NI (119.99 nm)", *J. Geophys. Res.*, **90**, 9845 (1985).

Ajello, J. M., Rao S. Mangina and R. R. Meier, (2011) "UV Molecular Spectroscopy from Electron Impact for Applications to Planetary Atmospheres and Astrophysics" Book **chapter 28**, published in "Charged Particle and Photon Interactions with Matter" Recent Advances, Applications, and Interfaces-Eds., Y. Hatano, Y. Katsumura, and A. Mozumder, Taylor & Francis, Boca Raton.

Ajello, J. M., C. P. Malone, J. S. Evans, G. M. Holsclaw, A. C. Hoskins, S. Jain, W. E. McClintock, X. Liu, V. Veibell, J. Deighan, J.-C. Gérard, and N. Schneider (2019). UV Study of the Fourth Positive Band System of CO and OI 135.6 nm from Electron Impact of CO and CO_2. *J. Geophys. Res. Space Physics*, **122**, 1-24, doi:10.1029/2018JA026308.

Ajello, J., C. Malone, W. McClintock, A. Hoskins, and R. Eastes, (2017) Electron Impact Measurement of the 100 eV Emission Cross Section and Lifetime of the Lyman-Birge-Hopfield Band System of N_2: Direct Excitation and Cascading, *J. Geophys. Res. Space Physics*, **122**, 6776-6790, doi:10.1002/2017JA024087.

Beegle, L., J. M. Ajello, G. K. James, D. Dziczek and M. Alvarez, "The emission spectrum of the CO ($A\ ^1\Pi - X\ ^1\Sigma^+$) Fourth Positive System by electron impact", *Astron & Astrophys*., **346**, 1 (1999).

Budzien, S. A., P. D. Feldman, and R. R. Conway, Observations of the far ultraviolet airglow by the Ultraviolet Limb Imaging experiment on STS-39, *J. Geophys. Res.,* 99, 23, 275-23, 287, 1994.

Cartwright, D., Vibrational populations of the excited states of N_2 under auroral conditions, *J. Geophys. Res.*, **83**, 517-531 (1978).

Eastes et al., Imaging the Boundary Between Earth and Space – A Preview of Space Weather Data from the Global-scale Observations of the Limb and Disk (GOLD) Mission, 2015 Space Weather Week, 13-17 April, abstract and invited presentation.

Eastes, R. W., and A. V. Dentamaro, Collision-induced transitions between the $a\ ^1\Pi_g$, $a'\ ^1\Sigma_u^-$, $w\ ^1\Delta_g$ states of N_2: Can they affect auroral N_2 Lyman-Birge-Hopfiled band Emissions, *J. Geophys. Res.*, ***101***, 26,931-26,940 (1996).

Eastes, R. W., Modeling the N_2 Lyman-Birge-Hopfield bands in the dayglow: including radiative and collisional cascading between the singlet states, *J. Geophys. Res.*, ***105***, A8, (2000) 18557-18573.

Eastes, R. W., W. E. McClintock, M. V. Codrescu, A. Aksnes, D. N. Anderson, L. Andersson, D. N. Baker, A. G. Burns, S. A. Budzien, R. E. Daniell, K. F. Dymond, F. G. Eparvier, J. E. Harvey, T. J. Immel, A. Krywonos, M. R. Lankton, J. D. Lumpe, G. W. Prölss, A. D. Richmond, D. W. Rusch, O. H. Siegmund, S. C. Solomon, D. J. Strickland and T. N. Woods (2008), Global-scale Observations of the Limb and Disk (GOLD): New Observing Capabilities for the Ionosphere-Thermosphere, "*Midlatitude Ionospheric Dynamics and Disturbances"*, *Paul M. Kintner Jr., Anthea J. Coster, Tim Fuller-Rowell, Anthony J. Mannucci, Michael Mendillo and Roderick Heelis, Editors.*

Eastes, R. W., D. J. Murray, A. Aksnes, S. A. Budzien, R. E. Daniell, and A. Krywonos, Modeled and Observed N_2 Lyman-Birge-Hopfield Band Emissions: A Comparison, *J. Geophys. Res*., doi:10.1029/2010JA016417 (2011).

Eastes, R. W., W. E. McClintock, A. G. Burns, D. N. Anderson, L. Andersson, M. Codrescu, J. T. Correira, R. E. Daniell, S. L. England, J. S. Evans, J. Harvey, A. Krywonos, J. D. Lumpe, A. D. Richmond, D. W. Rusch, O. Siegmund, S. C. Solomon, D. J. Strickland, T. N. Woods, A. Aksnes, S. A. Budzien, K. F. Dymond, F. G. Eparvier, C. R. Martinis, J. Oberheide (2017)**,** The Global-scale Observations of the Limb and Disk (GOLD) mission, *Space Sci. Rev.*, 212, pp. 383-408, 10.1007/s11214-017-0392-2.

Evans, J. S., et al. (2015), Retrieval of CO_2 and N_2 in the Martian thermosphere using dayglow observations by IUVS on MAVEN, *Geophys. Res. Lett.*, 42, doi:10.1002/2015GL065489.

Evans, J. S., D. J. Strickland, and R. E. Huffman, Satellite remote sensing of thermospheric O/N_2 and solar EUV, 2. Data analysis, *J. Geophys. Res.*, 100, A7, 12,227-12,233, JULY 1 (1995).

Freund, R. S., Radiative lifetime of N_2 ($a\ ^1\Pi_g$) and formation of metastable N_2 ($a'\ ^1\Sigma_u^-$), *J. Chem. Phys.*, **56**, 4344-4351 (1972).

Gilmore, F. R., R. R. Laher, and P. J. Espy, Franck-Condon factors, r-centroids, electronic transition moments, and Einstein coefficients for many nitrogen and oxygen band systems, *J. Phys. Chem*. Ref. Data, 5, 1005-1107, 1992.

Holland, R.F., Excitation of nitrogen by electrons: The Lyman-Birge-Hopfield system of N_2, *J. Chem. Phys., **51**,* 3940, (1969).

Herzberg, G., Molecular spectra and Molecular Structure I. Spectra of Diatomic molecules 1950, D. Van Nostrand Co. Inc. Toronto, Canada.

Heays, A. N., J. M. Ajello, A. Aguilar, B. Lewis, and S. T. Gibson, "The high resolution EUV spectrum of N_2 by electron impact," *Ap. J. Supp.*, **211**, 1-27 (2014).

Kanik, I., C. Noren, O. Makarov, P. Vatti Palle, J. Ajello and D. Shemansky, Electron Impact Dissociative Excitation of O2. II. Absolute Emission Cross Sections of OI(130.4 nm) and OI(135.6 nm), *J. Geophys. Res.*, 108, E11, 51256, doi:10.1029/2000JE001423 (2003).

Katayama, D. H., A. V. Dentamaro, and J. D. Welsh, 'State specific electronic quenching rates for N_2 a $^1\Pi_g$(v=0) level from collisions with He, Ar, and N_2.

Lee, R. et al., 'Laboratory Aeronomy by Electron Impact of CO and CO_2 for Analysis of UV Observations of the Martian Upper Atmosphere', AGU abstract session P031 - Processes in the present-day Atmosphere of Mars, San Francisco (2019).

Loftus, A. and P. H. Krupenie, "The spectrum of molecular nitrogen", *J. Phys. Chem Ref data,* **6,** 113 (1977).

Makarov, O., I. Kanik, J. Ajello and C. Noren, Electronic Impact Dissociative Excitation of O_2. I. Kinetic Energy Distributions of Fast Oxygen Atoms, *J. Geophys. Res.*, ***108***, E11, 5125, doi:10.1029/2000JE001422 (2003).

Malone, C. P., P. V. Johnson, J. W. McConkey, J. M. Ajello, and I. Kanik. Dissociative Excitation of N_2O by electron impact, *J. Phys. B: At. Mol. Opt. Phys*., ***41***: doi10.1088/0953-4075/41/9/095201 (2008).

Malone, C. P., J. M. Ajello, A. C. Hoskins, W. E. McClintock, and P. V. Johnson, Electron Impact of CO, CO_2, and N_2 using the MAVEN IUVS Flight Spare, 68th Gaseous Electronics Conference (GEC), October 12-16, 2015, Honolulu, Hawaii, USA. (Bulletin of the APS, 60 (9), Abstract BAPS.2015.GEC.GT1.8, (2015).

Marinelli, W. J., W. J. Kessler, B. D. Green and W. A. M. Blumberg, The radiative lifetime of N_2 ($a\ ^1\Pi_g$,v=0-2), *J. Chem Phys.,* ***91,*** 701, (1989).

Mason, N. J. and W. R. Newell, Electron-impact total excitation cross-section of the a $^1\Pi_g$ state of N_2, *J. Phys. B: At. Mol. Opt. Phys.*, **20**, 3913-21 (1987).

McClintock, W. E., N. Schneider, G. Hosclaw, J. T. Clarke, A. Hoskins, I. Stewart, F. Montmessin, R. Yelle, and J. Deighan, (2015), 'the Imaging Ultraviolet Spectrograph (IUVS) for the MAVEN Mission', Space Sci. Rev., DOI 10.1007/s11214-014-0098-7.

Noren, C., I. Kanik, J. M. Ajello, P. McCartney, O. Makarov, W. McClintock, and V. Drake, Emission cross section of O I (135.6 nm) at 100 eV resulting from electon-impact dissociative excitation of O_2, *Geophys. Res. Lett*., 2001.

Stevens, M., J. Gustin, J. Ajello, J. S. Evans, R. R. Meier, A. J. Kochenash, A. W. Stephan, A. I. Stewart, K. Larsen, L. W. Esposito, W. E. McClintock, G. Holsclaw, B. R. Lewis and A. N. Heays, The production of Titan's ultraviolet nitrogen airglow, W., *J. Geophys. Res*., **116**, A05304, doi 10.1029/2010ja016284 (2011).

Stevens, M. H., J. S. Evans, J. Lumpe, J. H. Westlake, J. M. Ajello, E. T. Bradley, and L. W. Esposito, Molecular nitrogen and methane density retrievals from Cassini UVIS dayglow observations of Titan's upper atmosphere, *Icarus*, 247, 301–312 (2015).

Strickland, D. J., J. E. Bishop, J. S. Evans, T. Majeed, P. M. Shen, R. J. Cox, R. Link, and R. E. Huffman, Atmospheric Ultraviolet Radiance Integrated Code (AURIC): Theory, software architecture, inputs, and selected results, *J. Quant. Spectrosc. Radiat. Transfer*, **62,** 689 (1999).

Strickland, D. J., J. S. Evans, and L. J. Paxton, Satellite remote sensing of thermospheric O/N_2 and solar EUV, 1, Theory, *J. Geophys. Res.*, 100, A7, 12,217-12,226 (1995).

Strobel, D. F., R. R. Meier and D. J. Strickland, (1991), Nitrogen airglow sources: Comparison of Triton, Titan, and Earth, *Geophys. Res. Lett.,* **18**, 689-692.

Tilford, S. G. and W. M. Benesch, Absorption oscillator strengths for the $a'\,^1\Sigma_u^- \rightarrow X\,^1\Sigma_g^+$ and $a'\,^1\Sigma_u^-$ and $w\,^1\Delta_u \rightarrow X\,^1\Sigma_g^+$ transitions of molecular nitrogen, *J. Chem. Phys.*, **64**, 3370-3374 (1976).

Wilkinson, P.G., and R.S. Mulliken, Forbidden band systems in nitrogen. II. The $a'\,^1\Sigma_u^- - X\,^1\Sigma_g^+$ system in absorption, *J. Chem. Phys.,* **31**, 674-679, (1959).

Young, J. A., C. P. Malone, P. V. Johnson, J. M. Ajello, X. Liu, and I. Kanik, Lyman-Birge-Hopfield emissions from electron impact excited N_2. *J. Phys. B: At. Mol. Opt. Phys*., **43**, doi:10.1088/0953-4075/43/13/135201 (2010).

Table 1

Relative Electronic Band Emission Vibrational Intensities at 30 eV.

Vibrational v′-level	FC factor	Image-1			Image-3		
		Low pressure	Medium pressure	High pressure	Low pressure	Medium pressure	High pressure
0	0.043	0.040	0.038	0.037	0.087	0.068	0.061
1	0.116	0.114	0.112	0.108	0.135	0.142	0.144
2	0.171	0.167	0.168	0.163	0.179	0.178	0.173
3	0.183	0.183	0.181	0.177	0.177	0.170	0.165
4	0.160	0.157	0.160	0.163	0.136	0.141	0.147
5	0.122	0.126	0.127	0.131	0.097	0.102	0.114
6	0.083	0.091	0.091	0.098	0.066	0.077	0.073
Total	0.877	0.878	0.877	0.877	0.877	0.878	0.877

Table 2

Measured LBH Emission Cross Sections.

Energy (eV)	Total Emission Cross section (10^{-17} cm^2)	Direct Emission Cross section (10^{-17} cm^2)	Cascade Emission Cross section (10^{-17} cm^2)	Predissociation Cross section (10^{-17} cm^2)	Excitation Cross section (10^{-17} cm^2)
40	2.12	1.67	0.45	0.23	1.90
100	.79	0.54	0.25	0.08	0.62
200	0.54	0.38	0.16	0.05	0.43

480

List of Figures

Figure 1. The electron impact fluorescence spectra at 30 eV from N_2 for Image-1 and Image-3 at high gas pressure of 5×10^{-5} Torr with an electron beam current of ~80 μA. The radial glow pattern extends from beam center at 0 mm to 400 mm. IUVS-OEM optic axis in vertical position with respect to the electron beam is centered 30.48 cm (6 inches) above the electron beam axis for Image-3. The two spectra are normalized to the LBH *a*(3,0) band at 135.4 nm. The LBH v′, v″=0, 1, 2, … progressions for v′=0, 1, 2, 3, 4 are indicated in the figure.

Figure 2. A glow model composed of two lifetimes that is the best MLR fit of the glow data at 100 eV electron impact energy with (a) medium pressure and (b) high pressure, and an electron beam current of ~150 μA. The MLR ascertains two best-fit direct excitation lifetimes: for direct excitation (~50 μs) to the $a\ ^1\Pi_g$ state in green, and for cascade-induced excitation (~5000 μs) from the ($a'\ ^1\Sigma_u^-$ and $w\ ^1\Delta_u \rightarrow a\ ^1\Pi_g \rightarrow X\ ^1\Sigma_g^+$) states to the *a*-state in magenta. We show the best model regression fits for the two lifetimes in black for each glow. Both sets of glow patterns show that only Image-1 captures a direct excitation spectrum with termination of direct excitation photons in the model, shown in green, near 10 cm radial distance from the electron beam. The Image-3 glow pattern in the model, shown in magenta captures the cascade-induced LBH spectrum, which dominates from radial distances of 22.5–38.5 cm.

Figure 3. Top Panel: (Bottom abscissa, left ordinate) IUVS-OEM electron-excited 30 eV Image-1 laboratory spectra is centered on the electron beam axis at a radial distance of 0 cm from the electron beam at low (light green) and high (dark green) pressure. The spectra are normalized to the LBH *a*(3,0) band at 135.4 nm. The difference between the two spectra near 149 nm is due to pressure dependence of the N I 149.3 nm emission. (Top abscissa, right ordinate) Comparison of the v′-vibrational populations from a Franck-Condon based theoretical model (filled circles) [Loftus and *Krupenie, 1977; Ajello, 1970; Ajello and Shemansky, 1985; Heays et al., 2012*] with v′-vibrational populations from MLR fits to Image-1 spectra at low (open circles) and high pressure (green squares)

and an Image-3 spectrum at high pressure (blue squares). Vertical uncertainty bars for fitted v′-vibrational populations are included in the plot but are not readily evident because the signal-to-noise ratio of the laboratory measurements is large (see Section 4 and Figure 6).

Bottom Panel: (Bottom abscissa, left ordinate) IUVS-OEM electron-excited 30 eV Image-3 laboratory spectra at a radial distance of 30.48 cm from the electron beam for medium (dark purple) and high (light blue) pressure. The spectra are normalized to the LBH *a*(3,0) band at 135.4 nm. (Top abscissa, right ordinate) Comparison of the v′-vibrational populations from a Franck-Condon based theoretical model (filled circles; same as used for Fig. 3a) with v′-vibrational populations from MLR fits to Image-3 spectra at low (open circles), medium (diamonds), and high (squares) pressures.

Figure 4. The v′-vibrational populations from MLR fits to the sum of Images 1–3 spectra at high pressure (blue squares) at electron impact energies between 30–200 eV. As in Figure 3, uncertainties in the measured spectra are propagated through the MLR fit when obtaining v′-vibrational populations and their corresponding uncertainty estimates, which are shown as vertical bars in the figure (not readily evident).

Figure 5. Direct emission cross sections as a function of energy normalized at 100 eV to the average medium pressure absolute emission cross section from MLR fit to the glow pattern of Fig. 2 at 100 eV and from medium pressure absolute emission cross section *Ajello et al.* [2017] at 100 eV. We also show a comparison of the excitation function of this experiment to the direct LBH emission cross section measurements of *Ajello and Shemansky* [1985] and *Young et al.* [2010] normalized to the 100 eV direct emission cross section of 5.4×10^{-18} cm^2 of this measurement.

Figure 6. Statistical SNR used to determine the 100 eV emission cross sections in Table 2 and Fig. 5 plotted as the ratio of the summed total signal counts, less background counts, of the raw data in all 65 s frame intervals for each of the three images (364 in number for Image-1 at 100 eV medium pressure). This was acquired over eight-to-ten hours divided by the background noise defined as the square root of the sum of the squares of the standard

deviation of dark counts for each of the dark-acquiring frames and the standard deviation of light counts of signal for each of the 65 s light-acquiring frames described in *Ajello et al.* [2017, 2019].

Figure 7. (Bottom abscissa, left ordinate) GOLD observed spectra summed in 50 km tangent altitude bins covering 100–150, 150–200, and 200–250 km. The spectra are normalized to the LBH *a*(2,0) band at 138.3 nm. (Top abscissa, right ordinate) Comparison of the v′-vibrational populations from a Franck-Condon based theoretical model (filled circles; same as used for Fig. 3) with v′-vibrational populations from MLR fits to the GOLD observed spectra at altitude bins covering 100–150 km (squares), 150–200 km (diamonds), and 200–250 km (open circles).

554

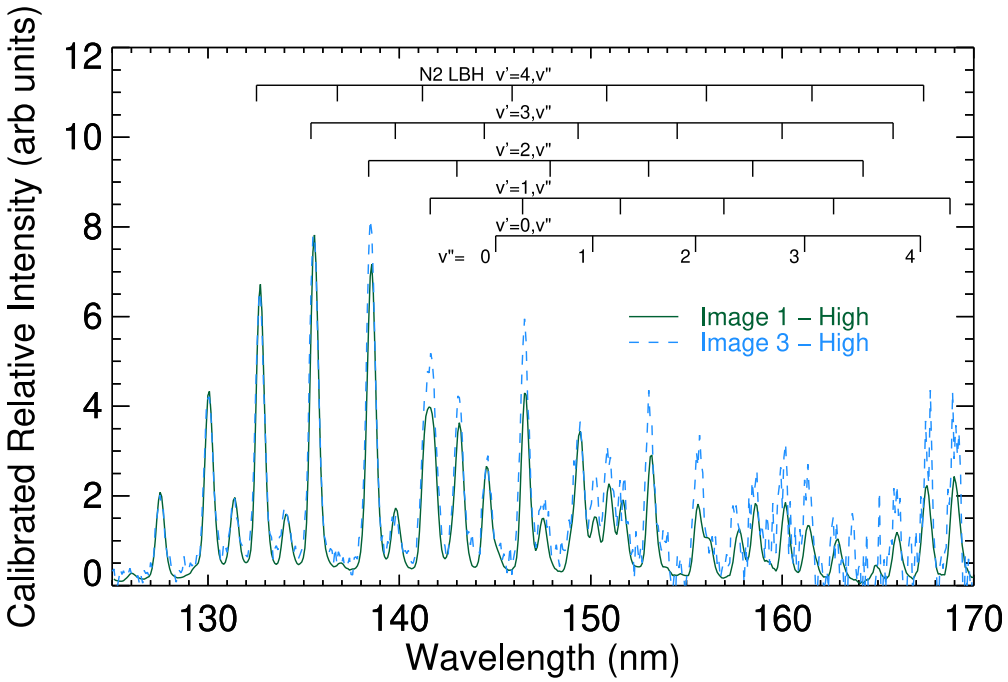

555
556 **Figure 1.**
557

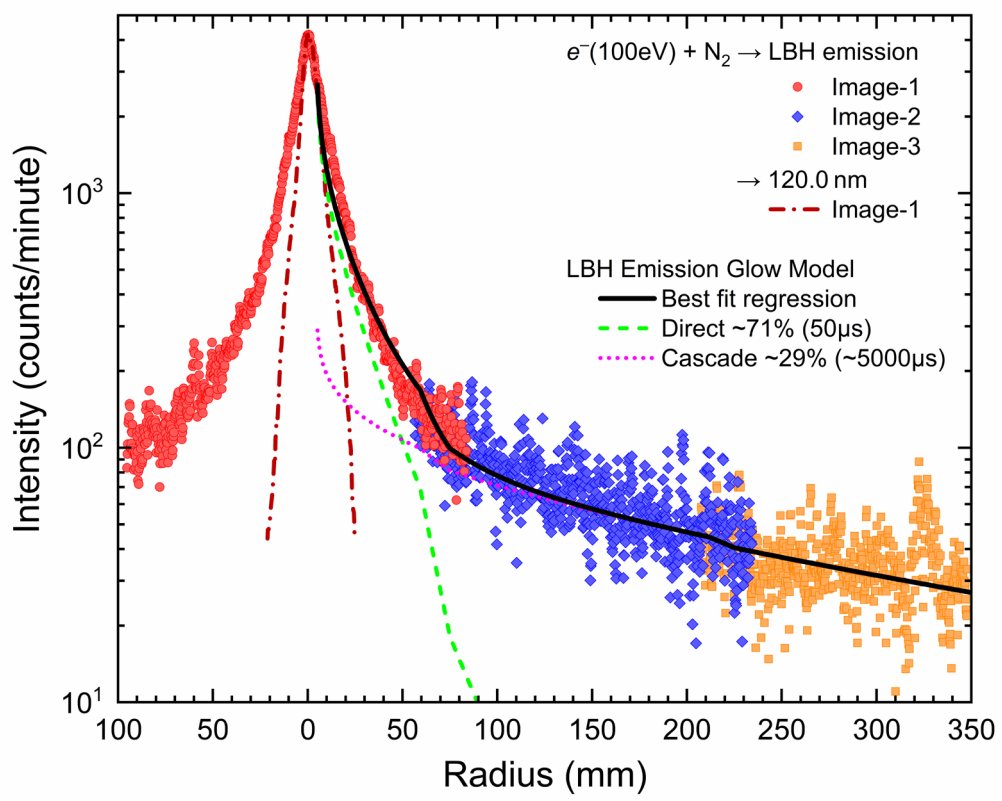
e^-(100eV) + N_2 → LBH emission
Image-1
Image-2
Image-3
→ 120.0 nm
Image-1
LBH Emission Glow Model
Best fit regression
Direct ~71% (50μs)
Cascade ~29% (~5000μs)
Intensity (counts/minute)
Radius (mm)

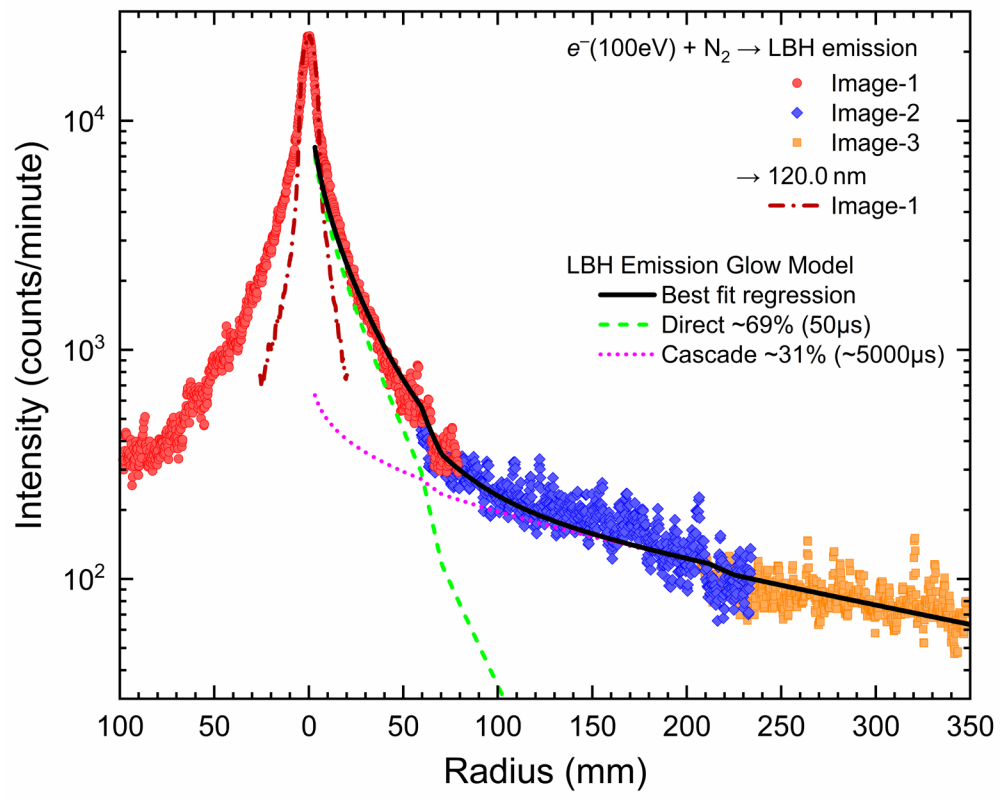
e^-(100eV) + N_2 → LBH emission
Image-1
Image-2
Image-3
→ 120.0 nm
Image-1
LBH Emission Glow Model
Best fit regression
Direct ~69% (50μs)
Cascade ~31% (~5000μs)
Intensity (counts/minute)
Radius (mm)

Figure 2.

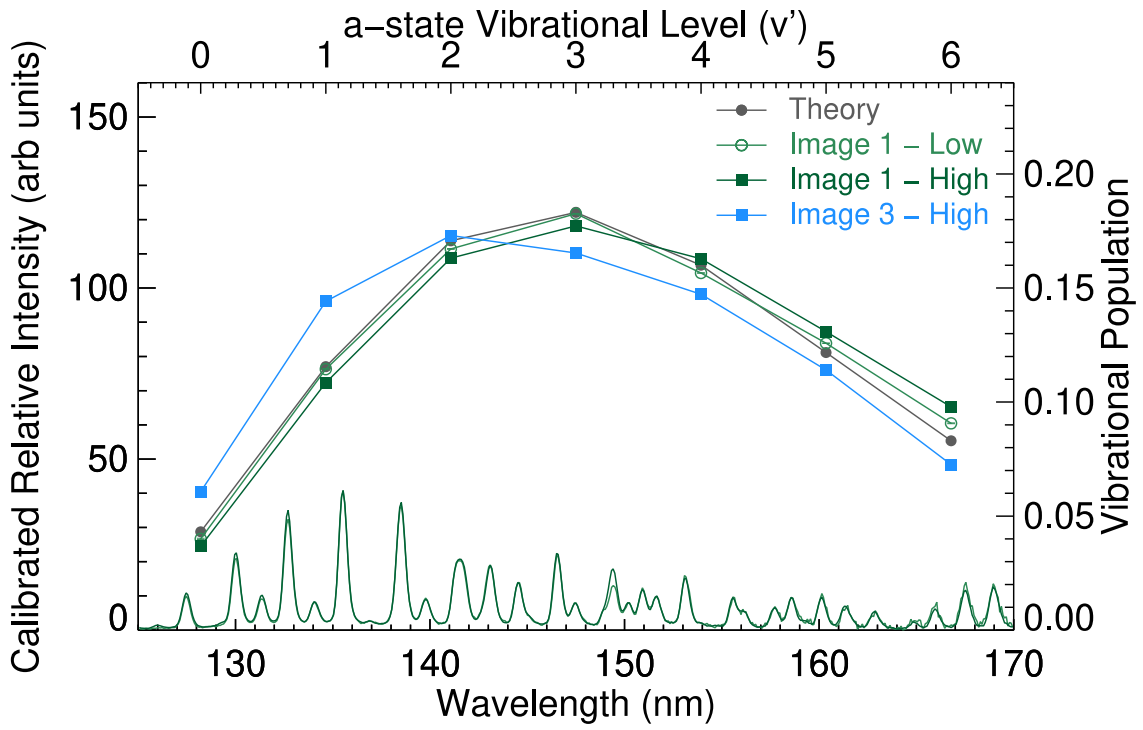

564

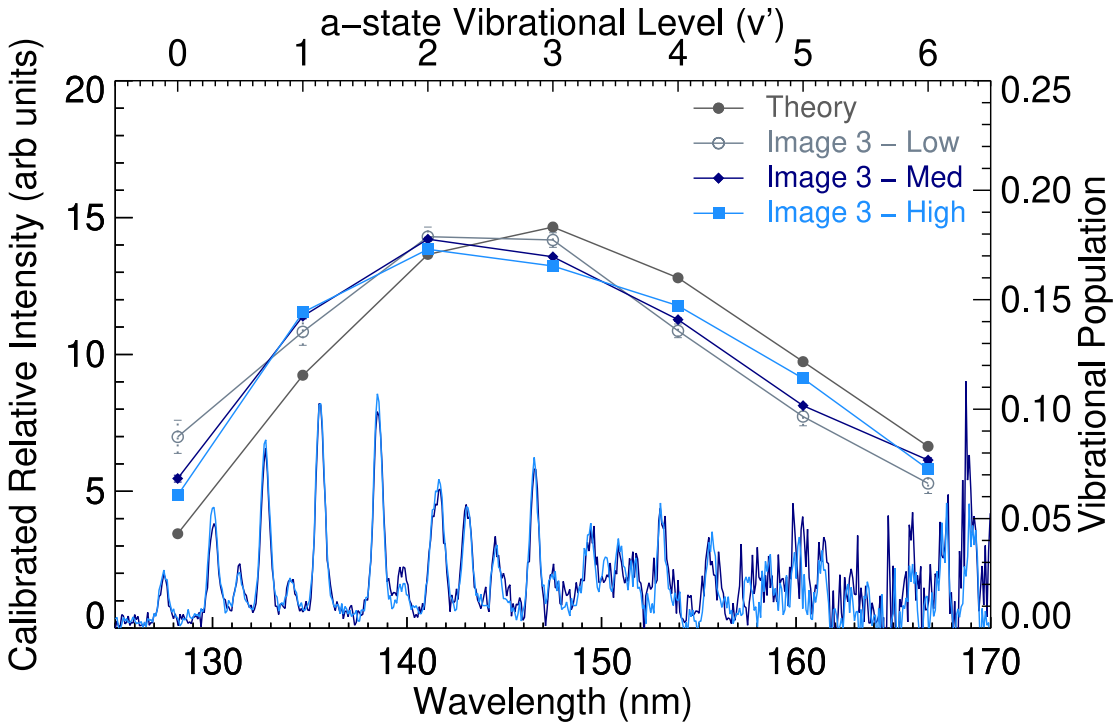

565
566

Figure 3.

567

568

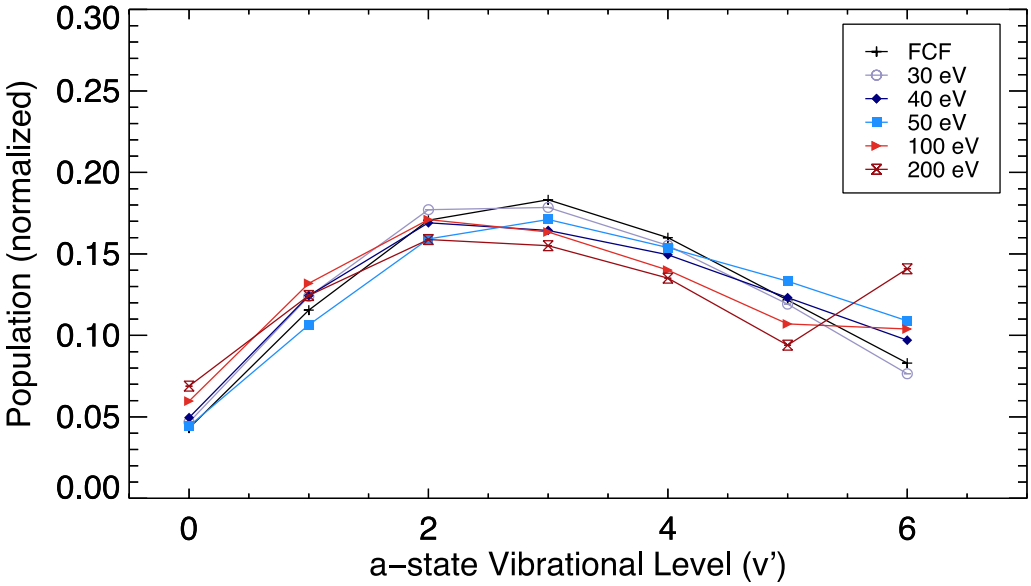

569
570
571 **Figure 4**
572

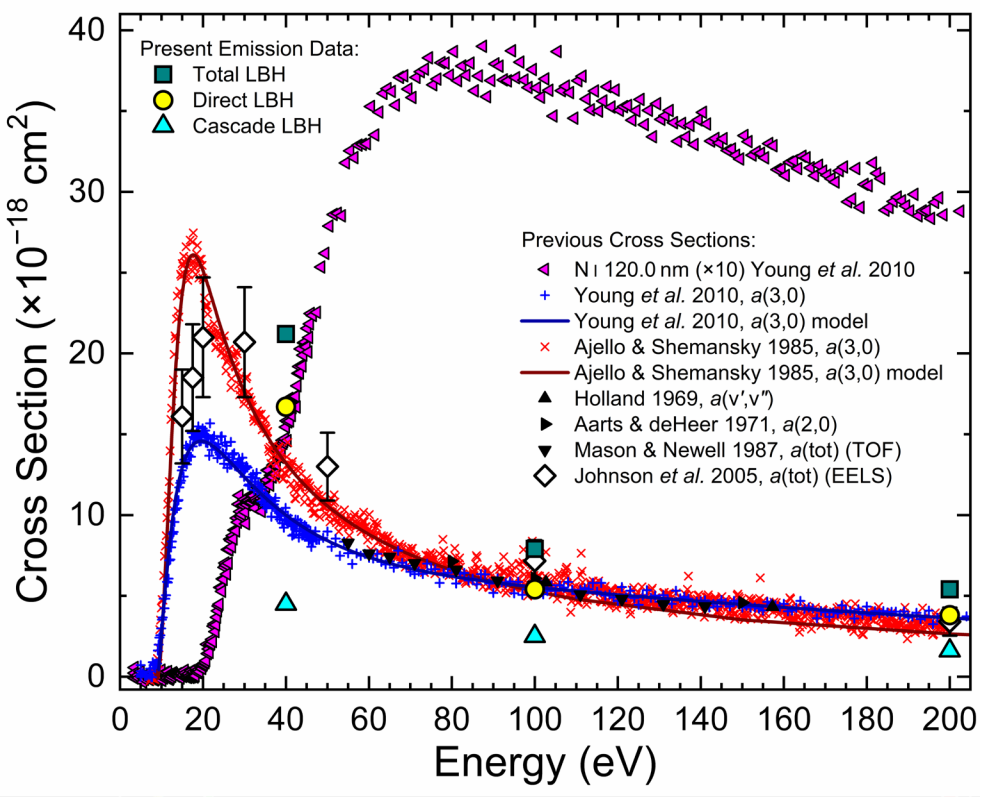
Present Emission Data:
Total LBH
Direct LBH
Cascade LBH
Previous Cross Sections:
N I 120.0 nm (×10) Young et al. 2010
Young et al. 2010, a(3,0)
Young et al. 2010, a(3,0) model
Ajello & Shemansky 1985, a(3,0)
Ajello & Shemansky 1985, a(3,0) model
Holland 1969, a(v',v")
Aarts & deHeer 1971, a(2,0)
Mason & Newell 1987, a(tot) (TOF)
Johnson et al. 2005, a(tot) (EELS)
Cross Section (×10^−18 cm^2)
Energy (eV)
0
10
20
30
40
0
20
40
60
80
100
120
140
160
180
200

Figure 5.

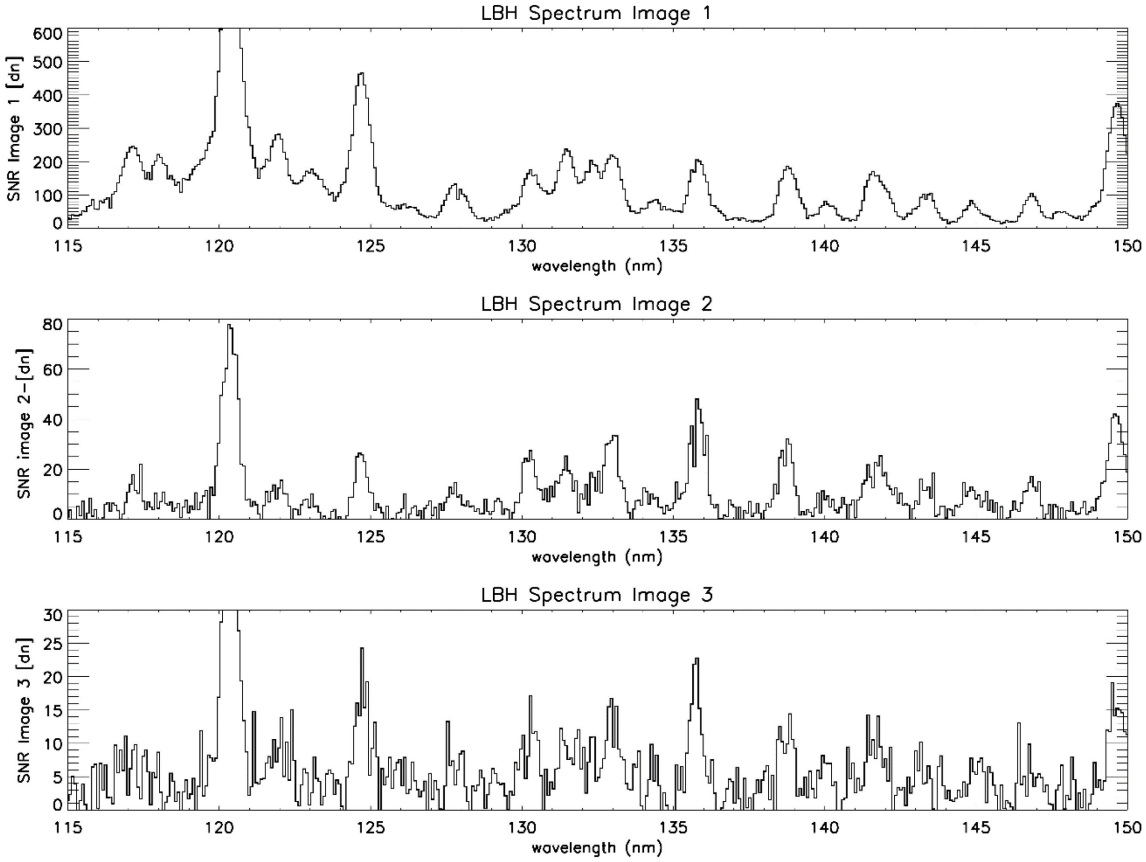
LBH Spectrum Image 1
SNR Image 1 [dn]
wavelength (nm)
LBH Spectrum Image 2
SNR image 2-[dn]
wavelength (nm)
LBH Spectrum Image 3
SNR image 3 [dn]
wavelength (nm)

Figure 6.

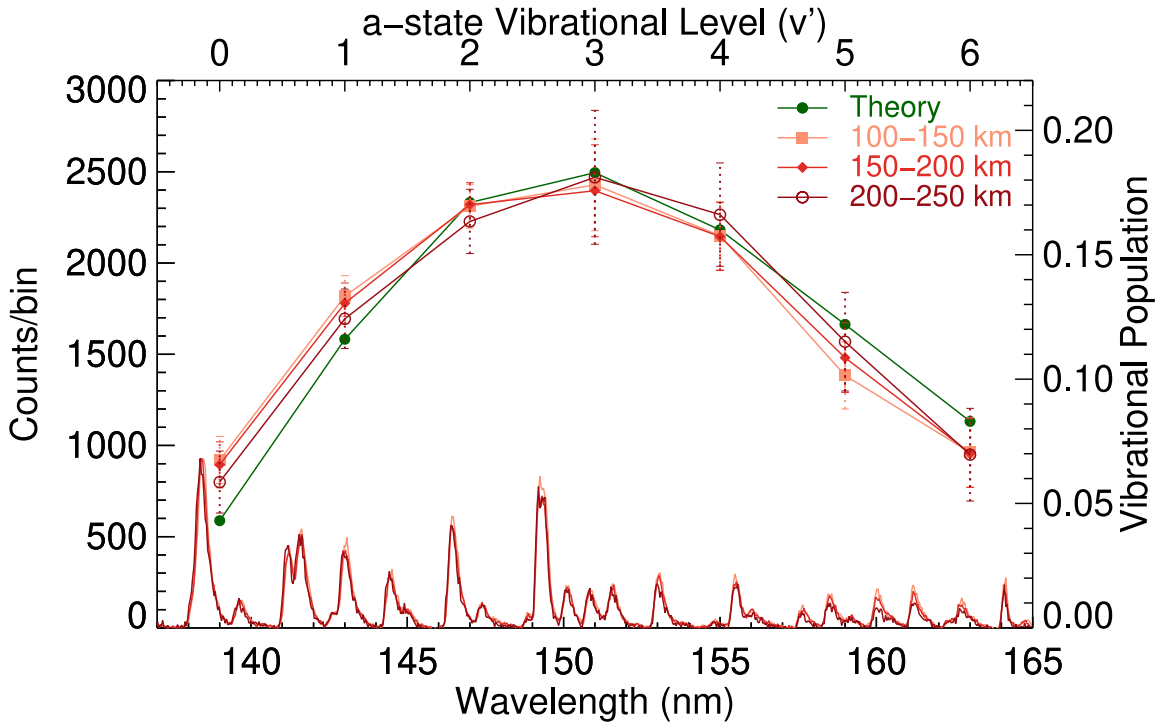
a–state Vibrational Level (v')
0
1
2
3
4
5
6
Theory
100–150 km
150–200 km
200–250 km
Counts/bin
Vibrational Population
Wavelength (nm)
3000
2500
2000
1500
1000
500
0
0.20
0.15
0.10
0.05
0.00
140
145
150
155
160
165

Figure 7.